MDPI

A Tribological Investigation of the Titanium Oxide and Calcium Phosphate Coating Electrochemical Deposited on Titanium

Adriana Santos [1], Jean Teixeira [1], Carlos Fonzar [2], Elidiane Rangel [3], Nilson Cruz [3] and Paulo Noronha Lisboa-Filho [2,*]

[1] Materials Science and Technology Program, Department of Physics, School of Sciences, UNESP—São Paulo State University, Bauru 17033-360, SP, Brazil
[2] Department of Physics, School of Sciences, UNESP—São Paulo State University, Bauru 17033-360, SP, Brazil
[3] Department of Control and Automation Engineering, Institute of Science and Technology, UNESP—São Paulo State University, Sorocaba 18087-180, SP, Brazil
* Correspondence: paulo.lisboa@unesp.br

Abstract: Titanium (Ti) and its alloys are widely used in biomedical applications due to their excellent mechanical properties and biocompatibility. However, they are a concern due to the possibility of cytotoxic effects coming from the degradation products. This degradation occurs by the combined action of corrosion and mechanical wear of these materials, which are released in the biological environment by the biomaterial implanted. The present article aims to investigate a new route to improve electrochemical and tribological performance with surface modification. Regarding the deposition of a protective layer on the surface, it consists of titanium oxide (TiO_2) and calcium phosphate (CaP). Both coatings were performed by chronoamperometric methods with titanium oxidation at 1 V and calcium phosphate reduction at -1.5 V. The corrosion and tribocorrosion tests demonstrated the effective combination of TiO_2 and CaP layer to protect the Ti substrate. Furthermore, this coating combination reduced corrosion degradation and mechanical wear in PBS, simulating a physiological environment. Additionally, it was observed that this combination of coating decreased the dissipated energy, and consequently, the wear decreased during sliding tests. All these findings indicate the protective behavior of the TiO_2 and CaP layer during the tribocorrosion tests.

Keywords: electrochemical deposition; corrosion; tribocorrosion; wear resistance; energy dissipation

1. Introduction

Titanium and its alloys are used widely in several fields due to its exciting combined properties being applied in the automotive industry as brake pads and connectors in rods [1,2], in aerospace as engine parts and airplane structures [3–5], and in biomedical applications as hard tissue substitute, including implants and prosthesis [6–8]. This versatility is attributed to its noble mechanical properties, low young modulus, low density, corrosion resistance, and biocompatibility [9,10], making titanium and its alloys preference choices, especially in medicine.

Despite its researche of appreciative properties, the process related to biomaterial can be challenging when applied in the biological environment. Furthermore, the literature indicates some clinical concerns about its long-term application, mainly due to low tribocorrosion resistance, lack of bioactivity, and risk of infection [11]. This challenge makes researchers pursue ways to overcome these concerning points, especially the interactions between corrosion and wear of titanium materials.

Many approaches have been proposed to improve bioactivity, tribocorrosion, and the synergism between corrosion degradation and mechanical wear. For example, the incorporation of titanium dioxide on the surface has been developed to improve bone formation in a faster and upgraded osseointegration process [12]. In addition, surface modification has a noble electrochemical behavior on biological fluids.

Different methodologies have been studied to promote the formation of a titanium oxide layer on titanium alloys. For instance, Trino and coworkers [12] obtained TiO$_2$ layers using the sol-gel approach with further incorporation of organic molecules, enhancing the biocompatibility, bioactivity, osteogenic capability, electrochemical, and mechanical aspects of these functional materials, thus obtaining significant improvement on corrosion and tribocorrosion performance.

On the other hand, different methodologies produce electrochemically oxidized TiO$_2$ layers by applying an electrochemical potential between titanium and counter electrodes [13–16]. These processes can produce high-quality ordered surfaces with insulating properties and possibilities to customize the process parameters with further incorporation of other compounds.

Other promising compounds to improve titanium surface properties are calcium phosphate (CaP) species, synthetic materials that can improve cell growth and differentiation and improve implant bioactivity. In addition, the modifications at the material surface reasonably support new bone formation for practical medical application [17,18].

The pulsed electrochemical deposition, a variation of the continuous electro nucleation process, has been demonstrated as a suitable methodology to achieve corrosion resistance coatings, decreasing ion release, and promoting apatite formation in NiTi alloys, according to Tohidi and coworkers' findings [19].

In solo performance or combination with electrochemical routes, inorganic coatings impact titanium's electrochemical and biological properties and alloys. The possibilities include the incorporation of calcium and phosphorous elements during plasma electrolytic oxidation [20], the combination of anodization with continuous chronoamperometry [21], or anodization and plasma electrolytic oxidation [22]. The combination of TiO$_2$ and CaP improves the inner-corrosion resistance of titanium dioxide with the bioactivity of calcium phosphate compounds [21,22].

Current reseaches agrees with the application of multi-layer and composition on the titanium samples' physical and electrochemical performance, which indicates a way to overcome concerns about the implant's long-term issues, primarily about electrochemical decomposition. On the other hand, the effect of wear degradation on these coatings needs attention and more evidence.

In the mechanical interaction, the wear during material motion produces a progressive loss of weight with the release of compounds [23,24], which can be evaluated in different parameters like friction force, plastic deformation, sample and counterpart, hardness, applied load, and energy dissipation [24–26]. The last one is conceptualized as quantifying energy dissipation due to the friction resistance of surfaces moving across each other [27].

The use of wear information can help to better comprehend the biomaterial performance. In addition, the mechanical influence on the complex tribocorrosion events was observed, according to Vieira and coworkers [28]. The variation in dissipated energy yields on the solution composition with the presence of corrosion inhibitors and the duration of wear test at the biological environment.

Another exciting finding using the concept of energy dissipation during tribocorrosion was obtained by Jahangiri and coworkers [27] using volumetric loss per energy dissipated, the parameter that can comprise an effective tool to compare materials during wear tests.

Following the reported approaches to overcome the complexity of titanium-based materials in the physiological environment, the present research proposal is to investigate the tribological performance of a new route to obtain bombinated TiO$_2$ and CaP coatings using low-cost electrochemical setup, with a focus on understanding the wear degradation and the combination of both in tribocorrosion tests and the use of energy dissipation in the interpretation of mechanical events.

2. Materials and Methods

Four samples were prepared using metallographic techniques until 1200 mesh with silicon carbide sandpaper and were etched with Piranha solution for 2 h. The first one was

of pure titanium (CP-Ti G4) without coating, also named Ti. The second sample CP-Ti G4 coating with titanium oxide (TiO_2) was called Ti/TiO_2. The third sample was a CP-Ti G4 coating with CaP, known as Ti/CaP. Finally, the fourth sample, CP-Ti G4 coating with both TiO_2 and CaP, was identified as $Ti/TiO_2/CaP$.

2.1. Deposition

The TiO_2-coated samples were obtained using chronoamperometry, performed using a Metrohm Autolab potentiostat and the NOVA software in H_2O_2 solution (10% in *v/v* in water with 0.5 g of NaCl) for 1800 s in a three-electrode system, with titanium, platinum, and Ag/AgCl as working electrodes, counter electrodes, and reference electrodes respectively. The oxidation was carried out for 1800 s with 1 V against the reference electrode with 10% H_2O_2 solution and 0.5 g of NaCl. The TiO_2 deposition was performed on surfaces of titanium substrate being repeated on the three samples for the two conditions studied (Ti/TiO_2 and $Ti/TiO_2/CaP$).

In a similar method, calcium phosphate was deposited by the pulsed chronoamperometry technique in a solution of $CaCl_2$ 0.17 M + $(NH_4)2PO_4$ 0.10 M. The deposition was repeated 10 times at 50 °C in –1.5 V. It was conducted with the power turned on and off for 30 s and 60 s, respectively. CaP deposition was carried out on two distinct surfaces. Titanium substrate was coated with CaP on one surface to yield Ti/CaP. Another surface was titanium oxide, on which CaP was placed to produce $Ti/TiO_2/CaP$. This method was performed three times for each of the two cases studied (Ti/CaP and $Ti/TiO_2/CaP$).

Each of the four groups investigated had three samples. Corrosion was done on one of the samples. Tribocorrosion was performed on another sample. Finally, one sample was utilized to perform confocal, SEM, DRX, wettability, and nanoindentation tests.

2.2. Confocal Microscopy and Scanning Electron Microscopy

Confocal Microscope LEICA DCM3D was performed to analyze the topography. In addition, the samples were measured in confocal microscopy in six points at all samples to observe the roughness variation between peak and valley. Moreover, to quantify the wear track volume, confocal measurements were performed at six different points.

Furthermore, Scanning Electron Microscopy (SEM) brand by Carl Zeiss and model EVO-LS15 were used to observe the variation in the surface roughness, the formation of coatings layers, and to analyze the wear track.

2.3. Phase Composition

X-ray Diffraction (XRD) using a RIGAKU DMAX diffractometer was performed with Cu Kα radiation source (λ = 1.54 Å) working at 40 kV and 15 mA. Measured at a step size of 0.02°, time per step of 3 s, and angle (ω) of 3°. The setup was with a discrepancy slit of 1/4° in a θ–2θ arrangement.

2.4. Wettability Test

The wettability was performed using the sessile drop technique with a Ramé-Hart 100-00 goniometer and software provided by the system manufacturer. The measurements were taken using 3 μL drops of deionized water at room temperature and repeated 30 times for each sample.

2.5. Corrosion Test

Corrosion tests were carried out in one sample of each group to investigate the effect of natural corrosion on the coatings using PBS. The samples were placed at the bottom of the electrochemical cell configuration using a standard three-electrode. One of the electrodes is the sample used as the working electrode wrapped in 100 mL of phosphate buffer (PBS) solution with pH 7.4 human-environment simulated fluid, used for each sample as the electrolyte at the physiological temperature of 37 °C. The second electrode is a counter electrode made of platinum. The third one was Ag/AgCl as the reference electrode. The

electrochemical measurement was conducted by a Metrohm Autolab potentiostat using the NOVA software. The electrochemical protocol was based on previous work [29]. First, the open circuit potential (OCP) was performed for one hour to stabilize the samples in the electrochemical cell's specific conditions. Afterward, linear polarization ranged from -1 V to 2 V with a scan rate of 10 mV/s.

The corrosion potential (Ecorr), current density (Icorr), polarization resistance (Rp), and corrosion rate (CR) were obtained by the results from the NOVA software. In addition, the protection efficiency (PE) was obtained by the methodology of Çomakli et al. [30].

2.6. Nanoindentation Test

The mechanical properties of the electrodeposited films were performed in nanoindentation tests. Indentations were made in 25, 50, 100, and 150 nm depth at 20 points of each coated group sample, thus enabling the obtainment of the nano hardness (H) and modulus of elasticity (E).

2.7. Tribocorrosion Test

Tribocorrosion tests were carried out in one sample of each group to investigate the effect of coatings on the friction processes in the biological environment using PBS. The samples were placed at the bottom of the same corrosion electrochemical cell configuration. However, it was using a standard two-electrode. One of the electrodes is the sample used as the working electrode at the physiological temperature of 37 °C. The second electrode is Ag/AgCl as the reference electrode.

Regarding the mounting of the tribometer, it was designed to hold the alumina sphere 6 mm diameter against the sample facing upward and submitted under a 1.55 N load. At the beginning of the experiments, every sample was kept in 100 mL of PBS until open circuit potential (OCP) stabilization was reached. Then, the OCP was maintained without changing, and the sliding started with the dynamic friction applied for 1800 s. During the last step, the attrition between the alumina ball and the sample surface was used to determine the coefficient of friction (COF). Finally, after stopping the sliding, the passivation began until reaching the OCP stabilization.

2.8. Mechanical Energy Dissipation Measurement

The instantaneous power through the data from the tribocorrosion tests was calculated using Equation (1), where P, Fa, ω, and Rm are instantaneous power (mJ/s), friction force (N), angular velocity (rad/s), and average radius of the wear track (m), respectively. The P refers to the amount of energy dissipated per unit of time by friction between the counterbody (AlO$_3$—6 mm diameter) and the studied samples. The value of ω was fixed at 2 rad/s and was controlled and measured for a rotational motion sensor (RMS-PASCO: CI6538). The friction (Fa) was measured using a mechanical system with a force sensor (FS-PASCO: CI6537). While the sample rotated at a speed of 2 rad/s, the 6 mm diameter sphere (AlO$_3$) was fixed to the mechanical system that contained the force sensor. This way, a wear track with a radius Rm was made on the sample and subsequently evaluated. In addition, the temperature of the solution was kept and controlled at 37 °C.

$$P = Fa * \omega * Rm \tag{1}$$

The dissipated energy during the wear process was evaluated during the tribocorrosion tests in PBS. The interference of the coating deposition on total dissipated energy (E_T) was due to mechanical wear. This interference was calculated from the total energy dissipated according to Equation (2). E_T was calculated by integrating the curve power (P) from 0 to 1800 s [31].

$$E_T = \int_0^{1800s} P(t)dt \tag{2}$$

2.9. Volume Loss and Wear Rate of the Measurement of the Track

Confocal microscopy was used to measure the loss in volume through the profiles in the *x* and *z* axis after tribocorrosion and to investigate the wear tracks morphology. In addition, SEM was used to observe the presence of the third body after sliding.

The loss in volume, which is the total amount of material detached, was quantified according to Equation (3), where *V*, *Rm*, and *Am* are the volume loss (μm^3), wear track average radius of the sliding (2×10^3 μm), and cross-section wears track area obtained in the confocal microscopy (μm^2), respectively.

$$V = 2 * \pi * Rm * Am \tag{3}$$

The wear rate was determined using Equation (4), where *Wr*, *Vm*, and E_T are wear rate ($\mu m^3/J$), volume loss (μm^3), and Total energy (J). The wear rate is the *Vm* divided by E_T, as shown:

$$Wr = Vm/E_T \tag{4}$$

3. Results and Discussion

3.1. Deposition

Figure 1a presents the chronoamperometry profile of a sample oxidation shown in two steps during these 1800 s. The first step is a drastic decrease in current during the first 50 s due to the formation of a cohesive oxide layer according to Equation (5), described by [29]:
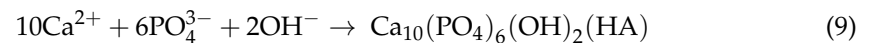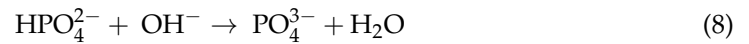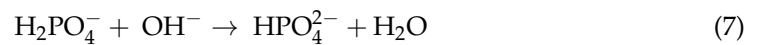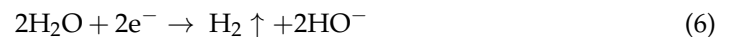
$$Ti + 2H_2O = TiO_2 + 4e^- + 4H^+ \tag{5}$$
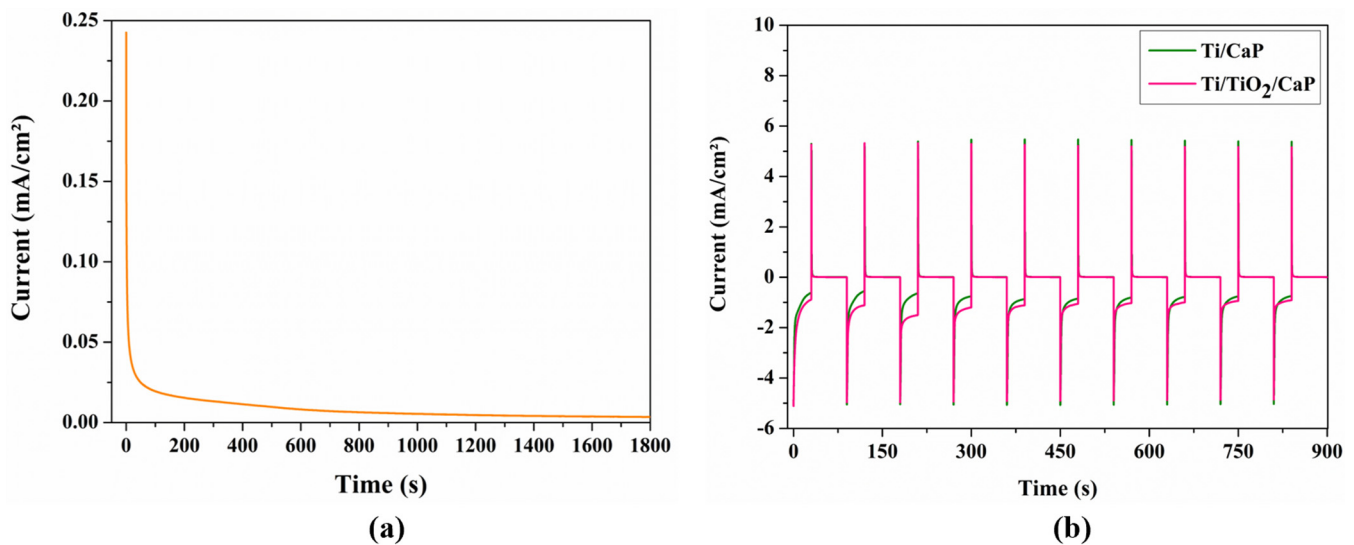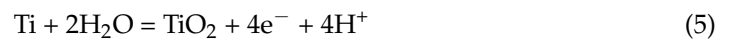
Figure 1. (**a**) Chronoamperometric graphs of titanium oxidation deposition. (**b**) Pulsed chronoamperometric graphs of calcium phosphate deposition.

In the second step, a rapid decrease in current can be observed, leading to a constant potential value. It is related to the interaction of both Ti^- and OH^- yielding on the surface of a TiO_2 layer during the superpotential application. In addition, this TiO_2 layer acts as a barrier to electron transfer at the cathode surface.

Figure 1b shows the pulsed chronoamperometry profile. It can be observed that in both cases, the current density reaches 5.0 mA/cm^2 in the applied potential. However, after turning off, it decreases quickly due to the adhesion of a resistive coating at the cathode surface promoted by the reduction of water molecules (Equation (6)) and phosphate-dehydration (Equations (7) and (8)) reactions as described by Li and coworkers [32]. These reactions induce a consequent increment of hydroxyl near the surface, promoting the increase of local pH and conducing to the calcium species precipitation. Afterward, the precipitated interact

with available phosphate groups to produce calcium phosphate compounds (Equation (9)) at the surface.

$$2H_2O + 2e^- \rightarrow H_2 \uparrow + 2HO^- \tag{6}$$

$$H_2PO_4^- + OH^- \rightarrow HPO_4^{2-} + H_2O \tag{7}$$

$$HPO_4^{2-} + OH^- \rightarrow PO_4^{3-} + H_2O \tag{8}$$

$$10Ca^{2+} + 6PO_4^{3-} + 2OH^- \rightarrow Ca_{10}(PO_4)_6(OH)_2 (HA) \tag{9}$$

The use of pulsed methodology has slight differences according to substrate pre-treatment. For example, in the Ti oxides samples, the current density always maintained a lower decrease rate compared to untreated samples, possibly due to de interference of the oxide layer on the compound deposition rate. This fact, accomplished with the power off time sequence, allowed a better ordination of calcium phosphate, preventing the shortage of calcium ions due to its consumption during power on stages and bubbles released from the surface, derivative of (Equation (6)) [33–35].

3.2. Confocal Microscopy and Scanning Electron Microscopy

Surface topography was evaluated using confocal microscopy to determine how the electrodeposition process affects the sample roughness. This parameter influences the interaction and attachment of the cell on the implant surface [36,37]. In addition, electrolyte penetration on the material is affected due to the distribution of valleys and pores [38].

Figure 2 shows the 3D profile topography image of the representative Ti uncoated surface (CP-Ti G4). All samples show regular topography, with uniform distribution of peaks and valleys, with arithmetic mean surface roughness (Ra) shown in Table 1, ranging from 274.95 ± 51.64 nm in the Ti sample up to 442.34 ± 40.86 nm on the Ti/TiO$_2$/CaP, and demonstrating the direct influence of the electrodeposition process in the final topography.

Regarding the different coating processes, the variation in the surface morphology is noticeable, with an increase in the Ra after compound deposition at the titanium surface, increasing from 398.27 ± 121.71 nm in CaP to 442.34 ± 40.86 nm in TiO$_2$/CaP. The inner differences in both electrodeposition processes can explain those values.
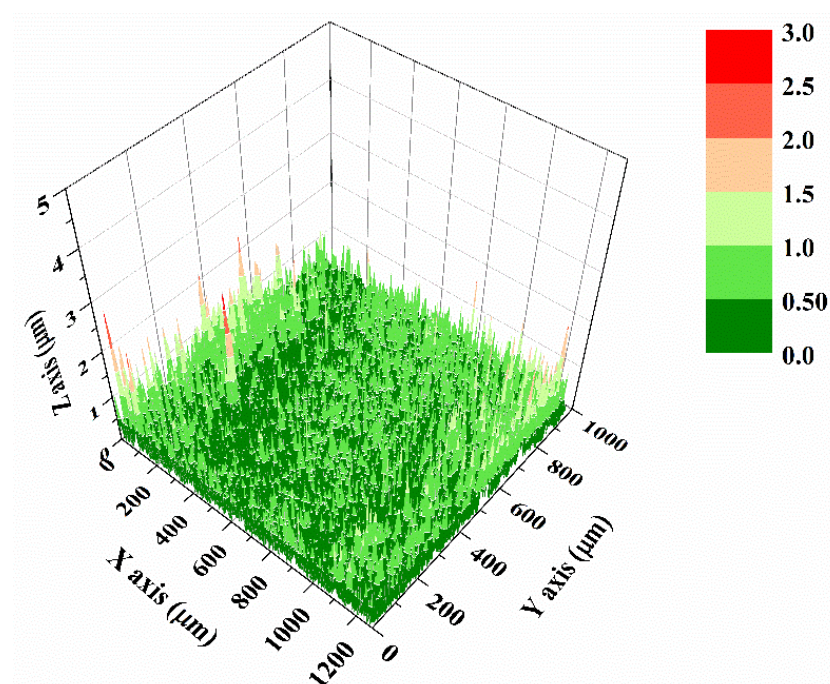

Figure 2. Confocal microscopy 3D profile representative topography of CP-Ti G4.

Table 1. Parameters obtained from confocal microscopy.

Sample	Roughness Ra (nm)
Ti	274.95 ± 51.64
Ti/TiO$_2$	436.61 ± 36.62
Ti/CaP	398.27 ± 121.71
Ti/TiO$_2$/CaP	442.34 ± 40.86

In the electrodeposition, the CaP reduction occurs at negative potentials, concurring with the hydrogen evolution, which can make the deposition of minor amounts of calcium phosphate compounds difficult, with a consequently limited variation of average surface roughness during deposition of hydroxyapatite on plasma electrolytic oxidated (PEO) titanium, asobserved by Zhang et al. [14].

On the contrary, the electrolytic formation of titanium oxide at anodic potentials is closely related to a significant variation in the Ra parameter [39,40], increasing the roughness due to the formation of the dense oxide layer, according to Equation (6). In addition, the promotion of anchoring sites to posterior CaP compounds [39] agrees with the change of Ra on Ti/TiO$_2$/CaP.

The variation in the surface roughness and the formation of coatings layers are corroborated by the distinctive rough areas observed by scanning electron microscopy in Figure 3.
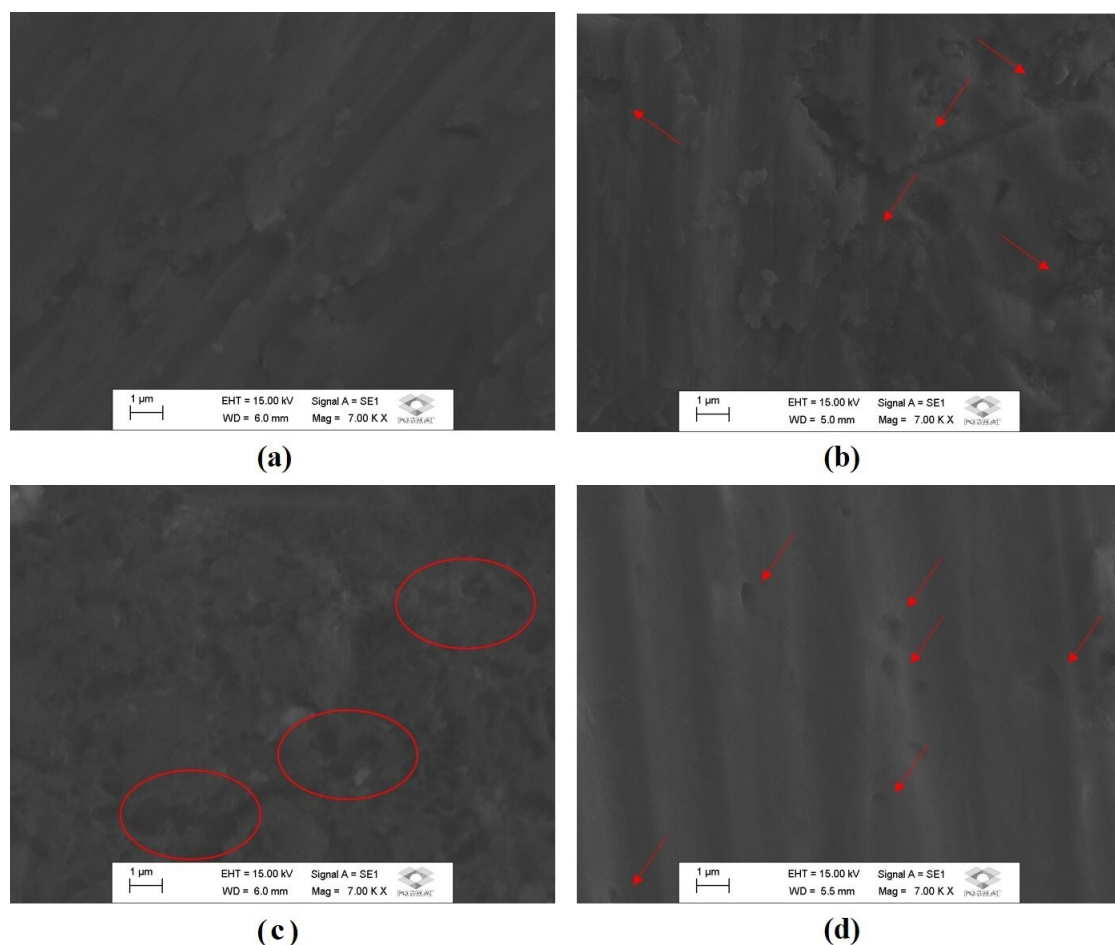
Figure 3. Scanning electron microscopy of (**a**) Ti (**b**) Ti/TiO$_2$ (**c**) Ti/CaP (**d**) Ti/TiO$_2$/CaP.

In Ti/TiO$_2$, the irregular areas are related to the formation of oxide on the titanium substrate, indicated by red arrows. While in the Ti/CaP sample, more dispersed areas with

tiny pores can be observed due to the concomitant titanium dissolution and calcium phosphate reduction at the titanium surface, indicated by red circles. Finally, the Ti/TiO$_2$/CaP sample presents a smooth surface with large cavities, contributing to the increase in the average Ra values observed in the confocal analysis.

3.3. Phase Composition

The X-ray diffraction technique was characterized to analyze the deposition process's effects on the formation of inorganic films. Its results are shown in Figure 4. It is possible to observe that the metallic substrate presents only peaks related to the alpha phase of titanium (JCPDS 01-089-2959), characteristic of CP-Ti G4 substrates.
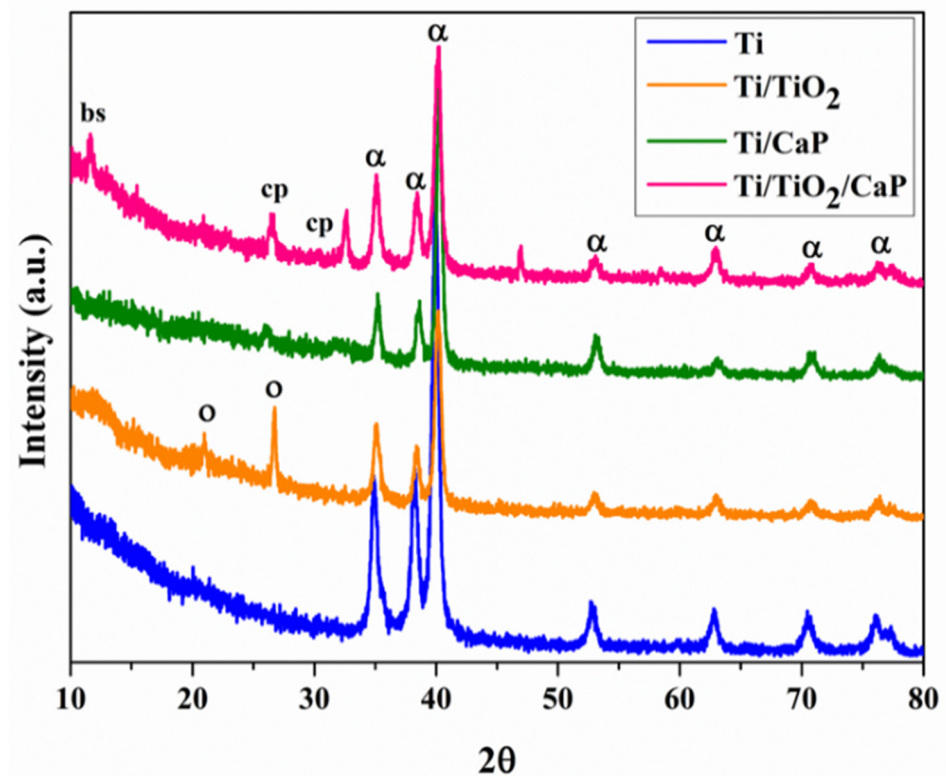
Figure 4. X-ray diffraction patterns of the samples studied.

After the different electrodeposition processes, it was possible to observe the formation of other crystalline phases according to the adopted methodology. For example, in the case of the sample coated only with titanium oxide (Ti/TiO$_2$), the formation of Ti$_3$O$_5$ phase (JCPDS 01-072-0519) occurred, which was stable at room temperature.

In the case of the sample with isolated deposition of calcium phosphate (Ti/CaP), the formation of a calcium phosphate hydroxide hydrate phase occurs, which is called Brushite (JCPDS 00-011-0293). In this sample, there was no perceptible phase of titanium oxide, thus indicating that the process effectively reduced calcium phosphate compounds on the surface of CP-Ti G4. This fact corroborated the variations observed through confocal and scanning electron microscopy.

Using a pre-coating of titanium oxide (Ti/TiO$_2$/CaP) made it possible to modify the deposited phases resulting from the calcium phosphate reduction. In addition, the previous presence of Ti$_3$O$_5$ enabled the interaction between the reduced calcium species and the available oxide, thus allowing the formation of calcium titanium oxide phase (JCPDS 01-082-0232). Additionally, in this configuration, there is also the formation of Brushite (JCPDS 00-011-0293), the calcium phosphate hydroxide hydrate phase, characteristic of deposition conditions of calcium phosphate in an acidic medium on titanium oxide [41].

Such evidence demonstrates the ability of new configurations of pulsed electrodeposition in multiple steps to obtain different crystalline phases from the same precursor solution.

3.4. Wettability Test

The contact angle tests were performed to find a relationship between the coatings and wettability and the results are exposed in Figure 5. Therefore, it can be observed in Figure 5a that both samples with CaP coating are the most hydrophilic among the four samples studied due to the contact angle of less than 90°, which means more excellent wettability (lower contact angle) [42]. On the other hand, the case of the sample with Ti/TiO$_2$ is the most hydrophobic due to the contact angle greater than 90°, which infers less wettability. Hence, Ti/TiO$_2$ surfaces showed the lowest wettability, followed by Ti, Ti/TiO$_2$/CaP, and Ti/CaP surfaces.
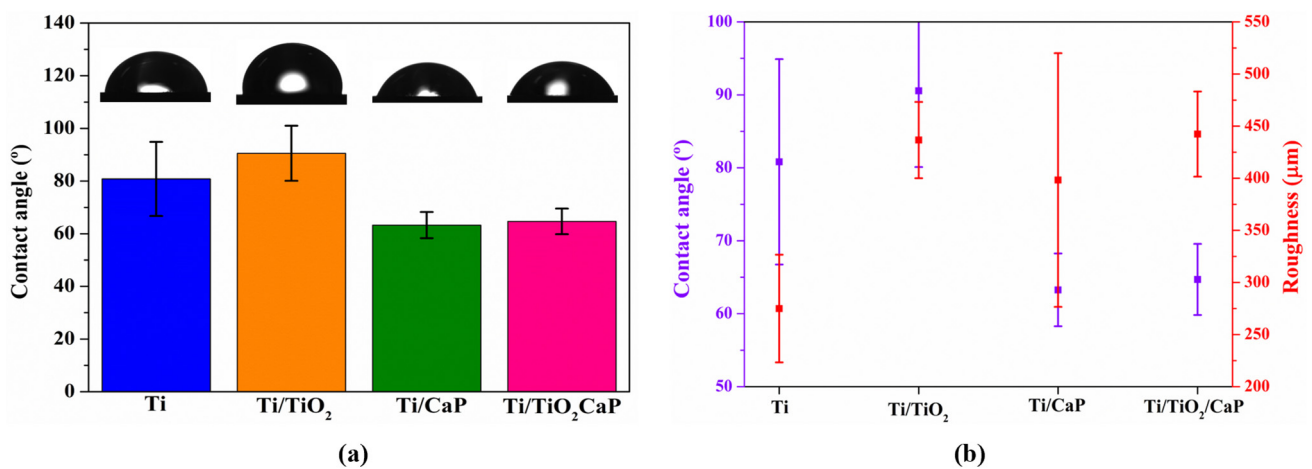
Figure 5. (**a**) Contact angle of analyzed sample groups. (**b**) Correlation between contact angle and roughness.

According to [43], the corrosion current density decreased and the corrosion potential increased due to rendering a surface superhydrophobic. Therefore, hydrophilic samples have a greater tendency to corrode faster due to their absorption of more fluids in comparison to hydrophobic samples. However, the corrosion results showed that the ones with TiO$_2$ formed a protective layer, thus preventing corrosion.

Rosales-Leal et al. (2010) [44] state that roughness strongly influences wettability; as the surface area increases with higher roughness, the measured contact angle decreases, becoming more hydrophilic. However, this statement can be misleading because the effect of roughness overshadows the influence of interfacial energetics.

In Figure 5b, it can be observed that, despite maintaining high roughness, both CaP alone and CaP with TiO$_2$ decrease the contact angle, becoming more hydrophilic when compared with the Ti/TiO$_2$. The hydrophilicity can enable more excellent cell anchoring, a requirement for biomaterials.

3.5. Corrosion Test

The deposition of calcium phosphate species isolated or combined with titanium oxides affected the corrosion behavior of CP-Ti G4 bulk on the electrochemical tests.

First, the open circuit potential was recorded during 3600 s in PBS, presented in Figure 6a, and the final OCP at the end of 3600 s is described in Table 2. It can be observed that the uncoated sample (Ti) presents the lower OCP, with a slight decrease in the first 500 s and posterior stabilization in –0.439 V. In contrast, all coated samples presented a similar behavior with a constant increase in the OCP value to the anodic direction, with the Ti/TiO$_2$ and Ti/TiO$_2$/CaP samples presenting positive values of 0.250 V and 0.058 V, respectively. A similar tendency can be observed in the Ti/CaP sample; however, despite the modest increase in the OCP, it continues in the negative value with −0.110 V.

(a)

(b)

(c)
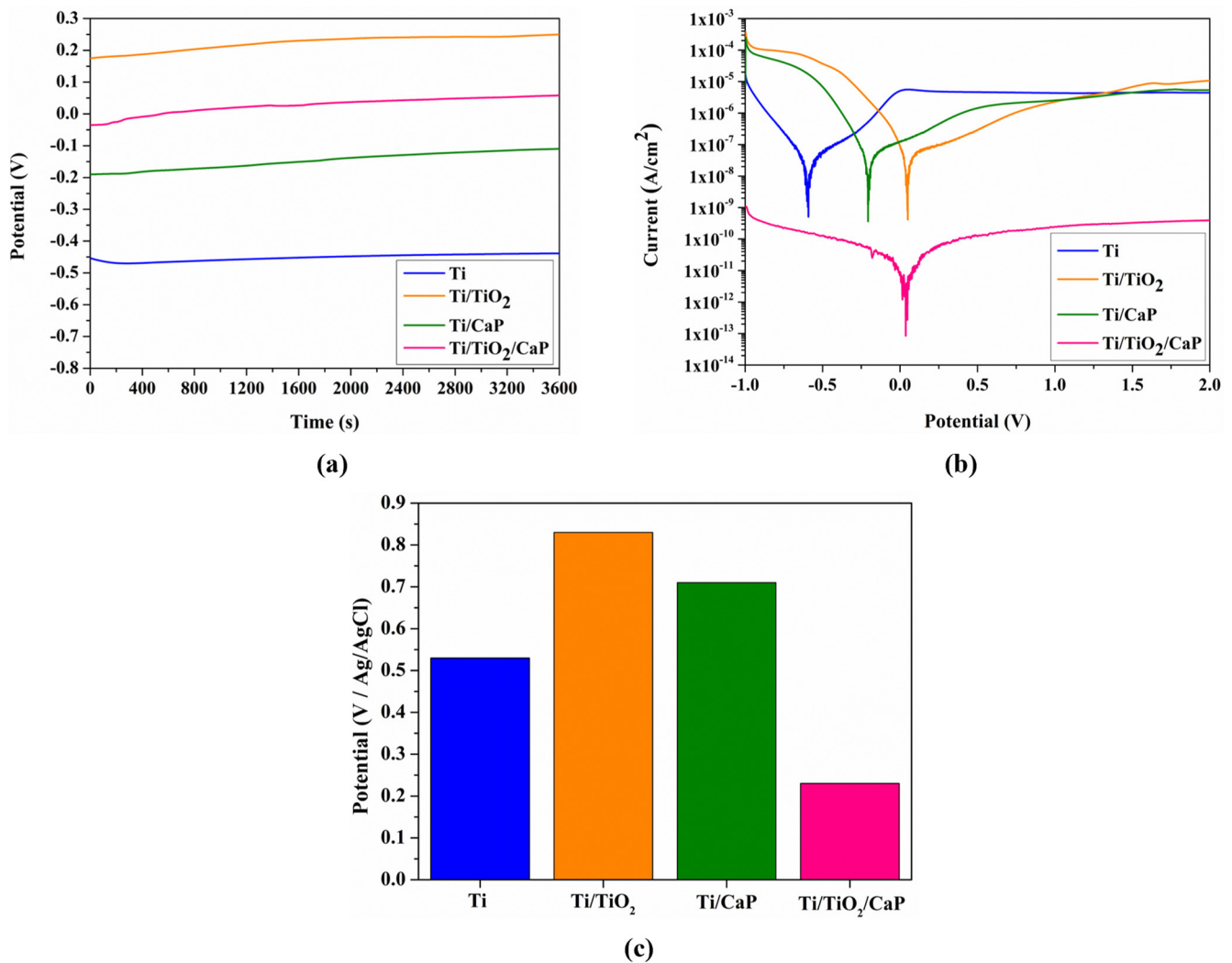
Figure 6. (**a**) Open circuit potential (OCP). (**b**) Linear potentialdynamic polarization. (**c**) Instability range in the cathodic region at the potentialdynamic polarization.

Table 2. Electrochemical parameters obtained from potentiodynamic polarization curves of studied alloys in PBS.

Sample	OCP (V)	Ecorr (V)	Icorr (A/cm^2)	Rp (kΩ·cm^2)	CR (mm/Year)	PE (%)
Ti	−0.439	−0.599	2.554×10^{-8}	1.100×10^3	9.5×10^{-3}	-
Ti/TiO$_2$	0.250	0.044	1.457×10^{-8}	8.351×10^2	3.8×10^{-3}	42.95
Ti/CaP	−0.110	−0.207	4.632×10^{-8}	6.075×10^2	15.3×10^{-3}	0 *
Ti/TiO$_2$/CaP	0.058	0.021	1.906×10^{-11}	3.641×10^6	6.3×10^{-6}	99.93

* There was no efficiency; on the contrary, there was an increase in the resistance current by 81.36%.

This impressive increase in the OCP of coated samples indicates the barrier effect attributed to inorganic species on the surface, which decreases the thermodynamic tendency to corrosion with the potential change to more positive values [13]. Furthermore, these results indicate a better performance of TiO$_2$/CaP coatings, compared with isolated CaP electrodeposited sample, but lower than only the TiO$_2$ group.

This finding can be explained by the titanium dissolution observed by Katic et al. (2019) [45] during the electrochemical deposition of calcium phosphate on the titanium surface, when the authors found irregularities in the deposition at low cathodic potential,

promoting the formation of tiny pores. When the calcium phosphate is deposited after titanium oxidation, this primary layer acts as a possible protection barrier against titanium degradation during the cathodic potentials but with a partial dissolution, explaining the difference between the isolated titanium oxide layer of Ti/TiO_2 and the multi composition coating of $Ti/TiO_2/CaP$ OCP, which decrease from 0.250 V to 0.058 V.

After establishing the open circuit potential of all samples, polarization tests were performed to analyze the variations in some critical parameters of coated titanium samples. As a result, the corrosion potential (Ecorr), current density (Icorr), polarization resistance (Rp), corrosion rate (CR), and protection efficiency (PE) are presented in Table 2 according to the data obtained from the polarization curve, displayed in Figure 6b.

The Tafel extrapolation data in Table 2 shows that the samples enhanced the corrosion resistance after the coating process, becoming nobler than pure titanium grade 4. Positive variation Ecorr can be explained because there is a decrease in the Icorr and CR and an increase in the Rp [42]. Figure 6b presents the current density in scale logarithm versus potential against Ag/AgCl reference electrode. It can be observed that one-step coated samples present the same behavior, with displacement in Ecorr to nobler potentials after CaP or TiO_2 electrodeposition, with higher values achieved by a titanium oxide film. Similar behavior to OCP was reported by Singh et al. [46], which was explained by the barrier protection due to the low conductivity of the inorganic compound [47], protecting the bulk material from ion dissolution in contact with electrolyte [12].

Even with the insulating behavior due to the low conductivity of calcium phosphate-related species, according to Fathyunes et al. [38], in this study, the Ecorr of Ti/CaP is lower than Ti/TiO_2. This behavior could be addressed to at least two possibilities. Firstly, cracks in the layer promote the solution electrolyte penetration [37]. The second possibility could be a consequence of the previous: when an electrolyte is in contact with the substrate, the CaP can act as a cathode, promoting the galvanic corrosion of titanium, leading to its dissolution [14].

Otherwise, when applied together, the combination of titanium oxide and calcium phosphate presented Ecorr as similar to the isolated titanium layer, with a significant decrease in the Icorr and passivation current due to a synergetic insulating effect of both ceramic compounds [48].

This group with $Ti/TiO_2/CaP$ presents significant benefits in corrosion protection, with the expressive variation of Rp when compared to the isolated CaP, raising four orders of magnitude coming from 6.075×10^2 kΩ·cm^2 in Ti/CaP, increasing to 3.641×10^6 kΩ·cm^2 in the $Ti/TiO_2/CaP$.

This high Rp makes electron transport difficult across the material surface, impacting the correlated Icorr and CR. These parameters are fundamentals to evaluate the electrochemical behavior of biomaterials and their perspective for use.

Regardless of Ti/CaP, it can be observed in Figure 6b that despite the insulating behavior of CaP inorganic compounds, increase in the electrochemical parameter is found when compared to Ti. Thus, the Ecorr and CR after coating electrodeposition show values of 4.632×10^{-8} A/cm^2 and 15.3×10^{-3} mm/year in Ti/CaP, and 2.554×10^{-8} A/cm^2 and 9.5×10^3 mm/year in Ti, respectively.

All these electrochemical parameter changes imply that the isolated CaP (Ti/CaP) electrodeposited in cathodic potentials at the titanium surface in pulsed chronoamperometry results in a more reactive surface, implying long-term damages due to titanium dissolution and loss of implant integrity [49–51].

With regard $Ti/TiO_2/CaP$, when compared to Ti/CaP, this double layer presents three orders of magnitude decreasing on the Icorr to 1.906×10^{-11} A/cm^2 and CR 6.3×10^{-6} mm/year. While on the Rp, there was an increase of up to 3.641×10^6 (kΩ·cm^2), promoting a four order of magnitude.

In addition, these achievements can be correlated with a protection efficiency, presented in Table 2, corresponding to the relationship between the Icorr of coated and uncoated samples. Furthermore, it can be observed, as in the other parameters, that there is

better performance of the double electrodeposition (Ti/TiO$_2$/CaP) with 99.93% protection. In contrast, the Ti/TiO$_2$ presented only partial protection of 42.95%. Therefore, with regard to Ti/CaP, it did not present protection efficiency.

One way to evaluate the coating refers to how fast it can stabilize. For example, Figure 6c shows the complete stabilization of protective oxide after Ecorr on the anodic side of the curve can be observed to be faster on the Ti/TiO$_2$/CaP sample, with 0.23 V, followed by Ti with 0.53 V, the Ti/CaP with 0.71 V and Ti/TiO$_2$ with 0.83 V.

Therefore, two-step coating deposition using an intermediate titanium oxide layer between the bulk and the CaP (Ti/TiO$_2$/CaP) achieved overall success.

3.6. Nanoindentation Test

When analyzing the mechanical behavior of the coatings deposited separately, it is possible to observe higher values in the Ti/TiO$_2$ sample, reaching in the first 25 nm of the coating values with nanohardness (H) and modulus of elasticity (E) of 5.6 ± 3.9 GPa and 133.7 ± 46.7 GPa, respectively. The mechanical values decay as the coating depth increases, transitioning to the substrate, assuming values in H and E of 2.4 ± 0.5 GPa and 83.6 ± 12.1 GPa, respectively, as shown in Figure 7 referring to H (Figure 7a) and E (Figure 7b).
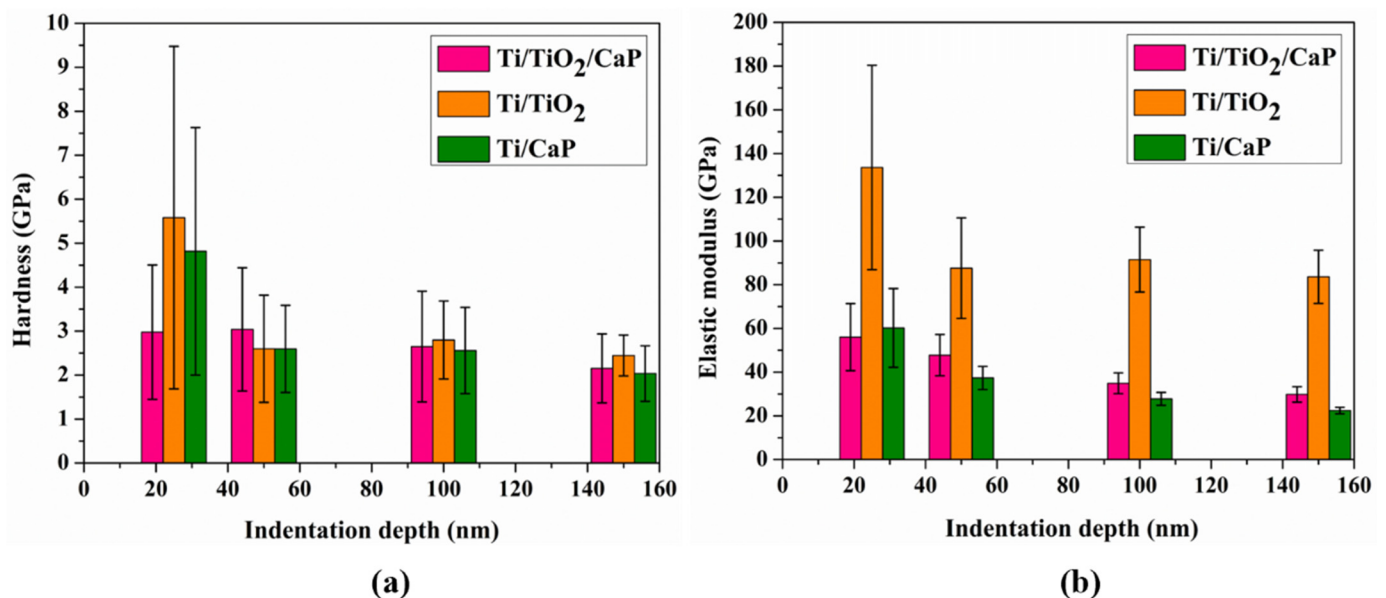
**Figure 7.** Nanoindentation tests: (**a**) Hardness. (**b**) Elastic modulus.

Similarly, the CaP-coated sample (Ti/CaP) shows higher H and E values in the first 25 nanometers of 4.8 ± 2.8 GPa and 60.2 ± 18.0 GPa, respectively.

When comparing both sample coatings with TiO$_2$ and Cap (Ti/TiO$_2$/CaP), the initial discrepancy in H values in this sample with the others Ti/TiO$_2$ and Ti/CaP in 25 nm were huge. However, the values changed due to the indentation depth was increasing, which both Ti/TiO$_2$ and Ti/CaP found to be similar in 150 nm, and the sample of Ti/TiO$_2$/CaP with 2.1 ± 0.6 GPa identical values considering the margin of erro. On the other hand, the value of E in 150 nm remained below that found for Ti/TiO$_2$, reaching 122.4 ± 1.5 GPa.

When using the double coating Ti/TiO$_2$/CaP, it was possible to observe an alteration concerning the individual values of H and E. Concerning H, this sample presented stable hardness values remaining below 3.1 GPa, starting with 2.9 ± 1.5 GPa in 25 nm depth, and reaching approximately 2.2 ± 0.8 GPa to 50, 100, and 150 nm of indentation depth.

3.7. Tribocorrosion Test

The tribocorrosion analysis was performed to evaluate the open circuit potential (OCP) variation and the coefficient of friction (COF) in concomitance, as shown in Figure 8. In addition, those results were associated with the synergism of electrochemical corrosion and mechanical wear.
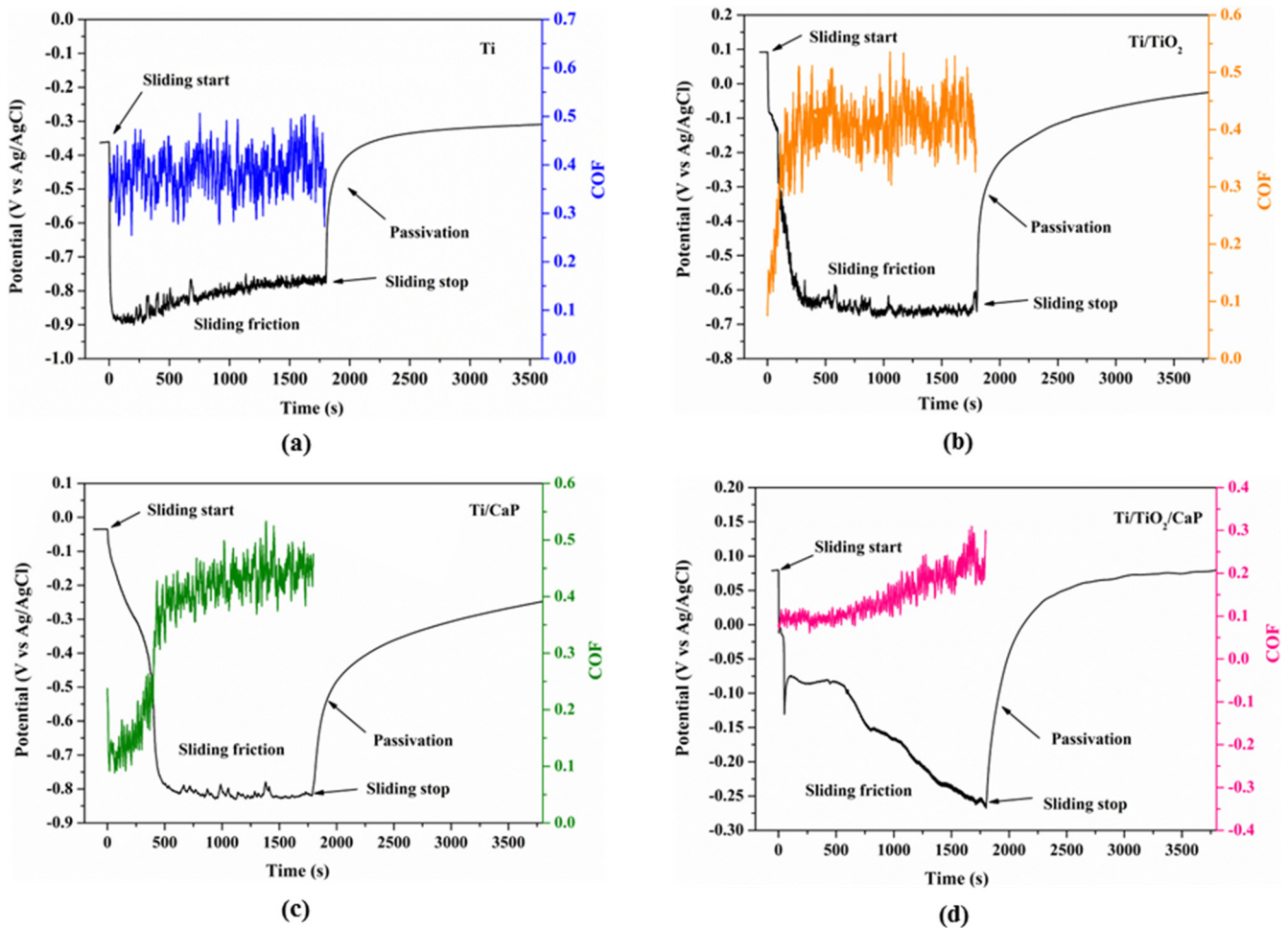
Figure 8. OCP and COF acquired during tribocorrosion tests in PBS. (**a**) Ti (**b**) Ti/TiO$_2$ (**c**) Ti/CaP (**d**) Ti/TiO$_2$/CaP.

Figure 8 shows significant differences between bare and coated samples in tribocorrosion tests. First, the bare titanium sample has only one potential decrease due to the sliding beginning. The potential falls to -0.9 V and increases until -0.8 V during the slide, following previous works evaluating titanium samples [47,51]. However, the coated samples presented decreased steps due to electrodeposited layers of the wear and electrochemical degradation.

The Ti/TiO$_2$ samples instantly decrease in open circuit potential with the sliding start and could be observed until 90 s, a slight and progressive decrease. After that, the sample presented another drop that begins at 100 s and until 220 s, stabilizing in the same potential as uncoated samples, which is characteristic of exposed titanium bulk. This step is probably attributed to the degradation of the amorphous TiO$_2$ layer, providing partial protection due to the successive compaction of thin-coating debris and its broke finishing in the bulk interface where OCP reaches a stable value [52].

Similarly, the Ti/CaP presents a graduate decrease in the potential during the first 400 s, during the transition of the CaP layer to titanium bulk, achieving a stable potential.

Regarding the coefficient of friction, an increase occurs until it reaches the characteristic values of metallic titanium.

Regarding the $Ti/TiO_2/CaP$, the OCP during tribocorrosion changed significantly. First, the instant decreased to -0.01 V, followed by another drop to -0.13 V. After, posterior decrease and stabilization on approximately -0.08 V until 530 s occur. Then, a permanent decrease in the OCP was observed in the sliding period until the potential of -0.26 V. In that group, the substrate OCP had not achieved all the $Ti/TiO_2/CaP$ sliding periods, producing evidence that the proposed coating promotes efficient protection against wear degradation.

Regarding the mechanical contribution to the degradation due to the friction between surfaces and consequent debris formation, the contribution can be analyzed using the coefficient of friction (COF). The concept is of the natural resistance to sliding between two surfaces on contact. In addition, the COF is directly proportional to the applied force and independent of the contact area [53]. Analyzing the OCP and COF data, it can be observed that electrochemical potential achieves a stable value related to the titanium response. The COF stabilizes at a medium value of 0.45, and those results were previously achieved by researchers in the literature [52,54].

The COF of about 0.45 is related to the contact between the sphere and the titanium bulk. Under this value, the COF corresponds to the sphere and the coating surface. Therefore, this parameter can evaluate the mechanical properties of electrodeposited TiO_2, CaP, and TiO_2/CaP layers. All the COF values were divergent after each electrodeposition method.

As observed in Figure 8, the COF remains stable during all experiments when having only a titanium substrate due to the inner resistance to the sphere slide on the material surface. However, in the coated samples, a transition occurs between the surface layer and the substrate wear response, increasing until a stable value of COF 0.45, similar to OCP variation.

In the Ti/TiO_2- and Ti/CaP-coated samples, the friction began with shallow values, approximately 0.1, corresponding to the lubricant layer character of amorphous TiO_2 and calcium phosphate deposited on titanium substrate, which increased according to the layer degradation in the case of isolated compounds. Otherwise, the $Ti/TiO_2/CaP$ presented a low COF during all the experiments, reaching 0.25, which corroborates the findings in the OCP variation due to the main interactions between the alumina and TiO_2/CaP interface during the experiments.

Tribocorrosion and electrochemical have three main results of the $Ti/TiO_2/CaP$ sample. One result is the promoted efficient barrier layers for titanium substrate dissolution. The second result is the significative wear resistance. The third result is a low OCP variation.

3.8. Mechanical Energy Dissipation Measurement

Figure 9 presents the instantaneous power (*P*) and open circuit potential (OCP). In the Ti sample, a homogeneous energy distribution was observed due to the uniform composition. Furthermore, it promotes a stable interaction on the metal-ceramic interface during the tribocorrosion period. Therefore, the Ti sample presents a variation in *p*-value between 1.5 mJ/s and 3.5 mJ/s minimum and maximum, respectively. This variation is possible due to the continuous formation of debris. Eventually, acting as a third body causes points to interact with both substrate and debris [55].

Otherwise, in the Ti/TiO_2 and the Ti/CaP sample, the *P* increases to the average of 3.5 mJ/s and 2.75 mJ/s, respectively. Therefore, the differences between the *P* of both samples are due to layer degradation with the sliding over time. In the $Ti/TiO_2/CaP$ sample, the tendency of *P* was increased until it slowly reached 2 mJ/s at the end of the friction. This value indicates a uniform interaction surface on $Ti/TiO_2/CaP$ sample that shows more acceptable wear performance with lower resistance to the sliding than bare Ti and isolated coated.

(a)

(b)

(c)

(d)
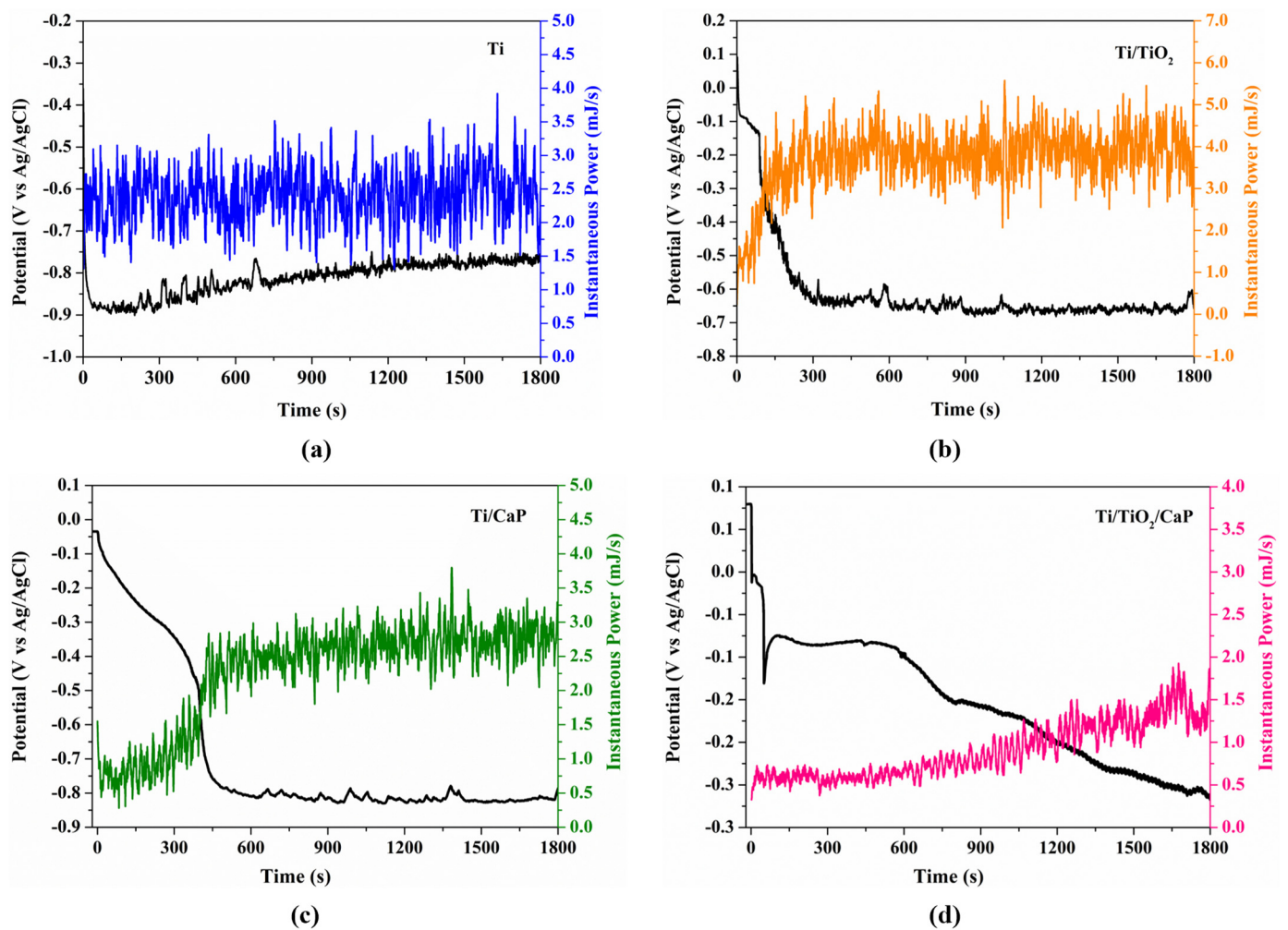
Figure 9. Instantaneous power and OCP evolution data obtained in tribocorrosion test (**a**) Ti (**b**) Ti/TiO$_2$ (**c**) Ti/CaP (**d**) Ti/TiO$_2$/CaP.

The coating efficiency was evaluated, assuming that the total contribution of *P* was due to the different three regions in the coated samples. The first region consists of the coating plateau, consistent with film interaction. The second region is the film/bulk interface when the *P* increase according to the OCP decrease. Finally, the third region is the contribution of titanium bulk, increasing to 1800 s.

Figure 10a shows the obtained data from the total amount of energy during the 1800 s and a comparative protection time due to coating response. The total amount of dissipated energy was compared in the four groups. There are visible significant differences in the sample coated with TiO$_2$ presenting a higher E_T. The E_T in the Ti/TiO$_2$/CaP sample decreased by 63.43% compared to Ti/TiO$_2$. The E_T variation can be associated with the total amount of *P* dissipated energy in contact with the double layer, which is approximately 0.5 mJ/s.

In Figure 10a, the first zone, called the film, is related to the period during the tests in which the coating supports the applied load. The second zone, called film/bulk, is associated with the period in which the beginning of coating degradation occurs consequentially to the fall of the OCP and increase in the *P*. Finally, the third zone, called bulk, is delimited by the stability of the OCP in values approximately -0.7 and *P* with values near the titanium without coating.
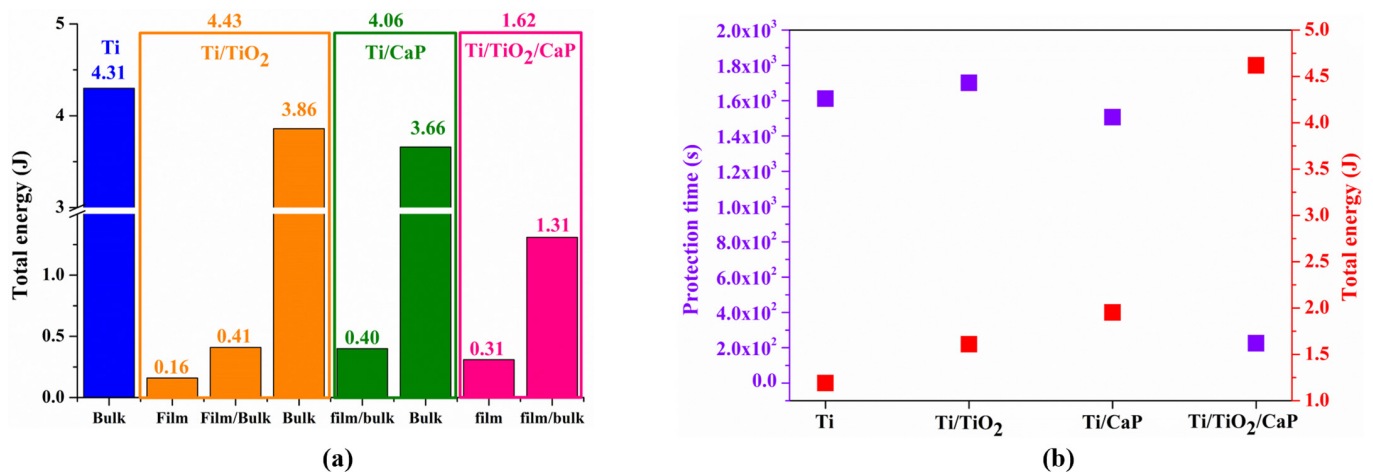
Figure 10. (**a**) Total dissipated energy during tribocorrosion (**b**) Correlation between total dissipated energy and protection time.

Comparing the *P* contribution into the different zones on the coated samples makes it possible to evaluate the individual impact on *P* and determine how these coating strategies perform in tribocorrosion.

In the Ti/TiO$_2$ sample, the film-attributed energy corresponded to 3.61% (0.16 J) in the first zone reaching up to 87 s. While in the second zone, the transition between coating and bulk that represented 9.26% (0.41 J) of the total energy during the slide reaches up to 220 s. Finally, 87.13% (3.86 J) of the substrate interaction with the alumina sphere reaches up to 1800 s in the third zone.

In the case of the Ti/CaP sample, it does not have a perceptible plateau of film interaction with the alumina sphere. Therefore, there is no first zone in this case. Instead, the film degradation event generates the electrochemical response with the gradation decrease of the OCP and mechanical response with the increase of *P*. This event reaches 400 s, representing 9.85% (0.40 J) of total *P* in the second zone. At the same time, the third zone remains 90.15% (3.66 J) to the substrate-sphere interaction until 1800 s.

Analyzing the strategies, in both cases of only one deposition layer, the transition zone represents about 9% (0.41 to Ti/TiO$_2$ and 0.40 to Ti/CaP) of total energy dissipated due to friction in PBS despite the difference in the interval period friction between 220 s to TiO$_2$ and 400 s CaP.

Finally, the Ti/TiO$_2$/CaP significantly reduces the total energy and the layer contribution. Therefore, there is no third zone in this case. Therefore, it was considered that all the energy dissipated was from interactions with the coating in the first zone representing 19.14% (0.31 J). In addition, the second zone has an energy demand of 80.86% (1.31 J), demonstrating the beneficial interaction of TiO$_2$ and CaP layers. These results show a protective effect of the synthesized coating.

In Figure 10b, the influence of the deposition process on the material can be associated with both times of protection and the total dissipated energy. The protection time corresponds to the synergism of surface interactions, mainly due to mechanical and electrochemical reactions. Total dissipated energy corresponds to the sliding resistance due to surface variations and coating interactions during the test.

In Figure 10b, a remarkable change in the protection time of each coating and the dissipated energy can be observed. Analyzing the *P* data, we can associate its decrease with the increased protection time. The Ti sample without coating did not show the resistance of the native oxide due to the COF and OCP that instantly stabilized. The isolated Ti/TiO$_2$ and Ti/CaP protection occurs with TiO$_2$ and CaP, attenuating the wear for 220 and 400 s, respectively. In the case of Ti/TiO$_2$/CaP, there was a significant increase in the protective resistance compared to isolated coating. This behavior confirms the primary response to better wear resistance on the coated materials.

3.9. Volume Loss and Wear Rate of the Measurement of the Track

During tribology tests, the material surface in contact with the alumina counterpart suffered degradation and presented a particular scar named, wear tracks. The specific interactions between the interfaces are correlated to the coating's electrochemical and tribological properties. These wear tracks obtained are presented in Figures 11 and 12.
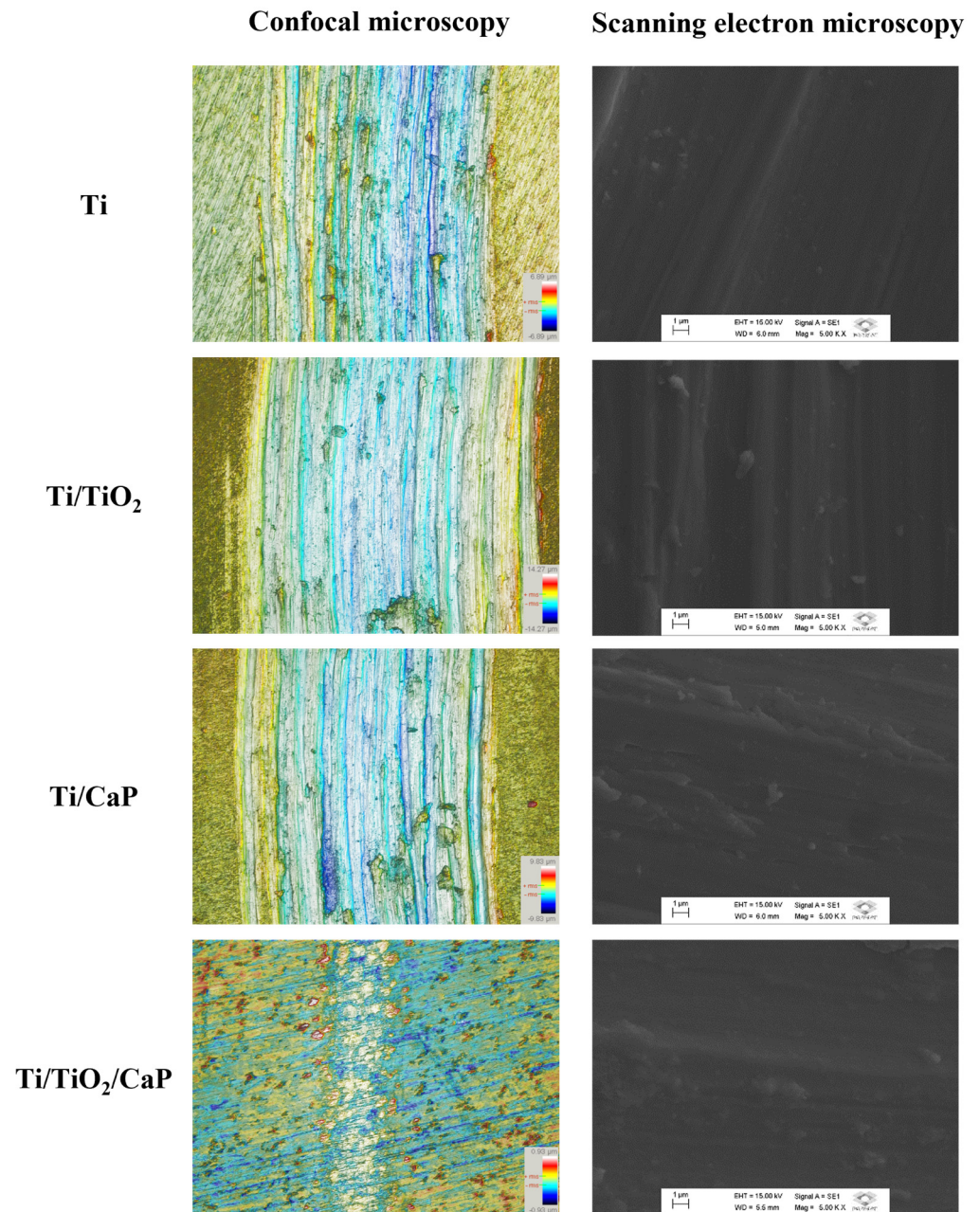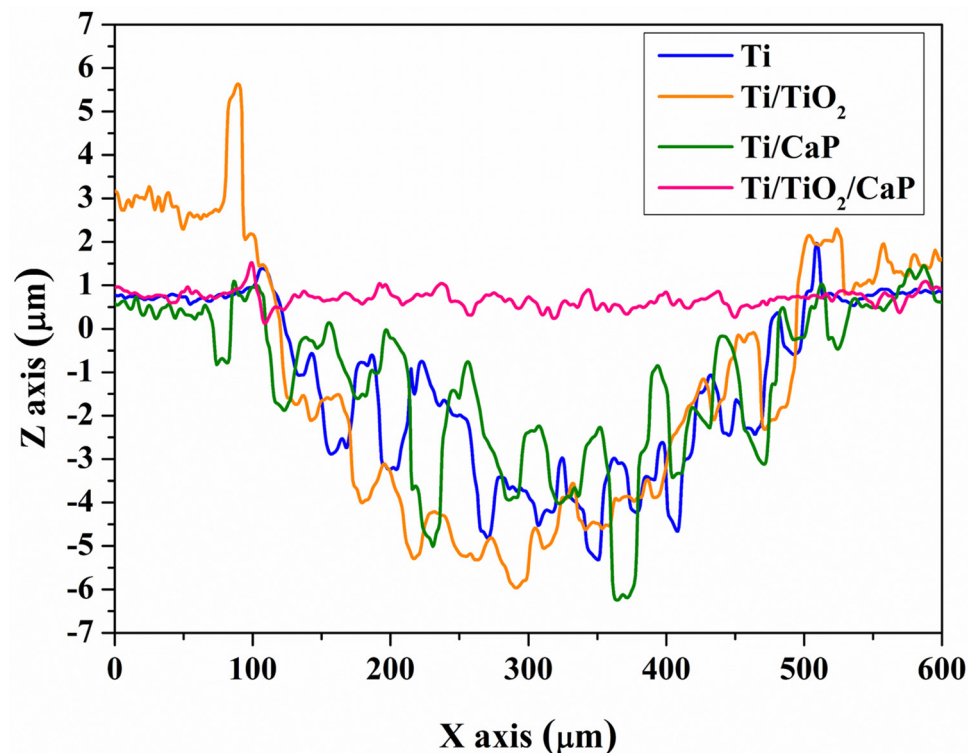
Confocal microscopy　　　**Scanning electron microscopy**

**Figure 11.** Confocal microscopy 2D profile of wear track and SEM.

Figure 12. Profiles in *x* and *z* axis of wear track after tribocorrosion experiments.

First, the pristine samples present a profile with a large and depth wear track. It is perceived as delaminated zones and an irregular contact surface due to the formation of hard-debris-trailed-forming grooves on contact scar. Due to the SEM image, it is possible to confirm that besides the same pattern scars, there is a presence of the third body. Second, on the TiO_2-coated samples, the tribocorrosion wear tracks present more prominent depth and large spots than all the rest. Third, pull-out zones can be observed due to the coating delamination and nonuniform corrosion degradation. The confocal analysis was confirmed with MEV images.

Third, on the CaP-coated samples, the tribocorrosion wear tracks were slimmer when compared with the TiO_2-coated samples. However, the CaP-coated surface shows a less homogenous surface among all samples in this study due to the formation of CaP that causes pitting on the titanium bulk even before wear tracking degradation. This phenomenon tends to rip out more pieces on the wear track than it is possible to realize on the confocal and MEV images due to the nonuniform surface and irregular scratches. This correlation of images agrees with the electrochemical analysis in which Ti/CaP samples present high CR.

Finally, on the $Ti/TiO_2/CaP$ sample, the tribocorrosion wear tracks were slimmer and smoother than all cases in this study, as could be realized on the 2D profile. There is minimal visible damage after sliding wear tests. This information of both confocal and MEV images corroborates with the minor variation in the OCP and greater passivation. In addition, the $Ti/TiO_2/CaP$ group can be observed with high protection against tribocorrosion and wear with a minor wear track zone. This pattern agrees with the protection efficiency on electrochemical tests and lowers *P*, corroborating the beneficial response of two deposition stages, promoting a more stable and resistant layer into titanium surfaces.

These observations were quantified in the volume loss graph in Figure 13a, where uncoated titanium has 4×10^3 μm^3 of volume loss. In comparison, samples with only TiO_2 and CaP increase the values to approximately 4.7×10^3 μm^3 and 4.9×10^3 μm^3, respectively. However, samples with TiO_2 and CaP 0.9×10^3 μm^3 decreased drastically.
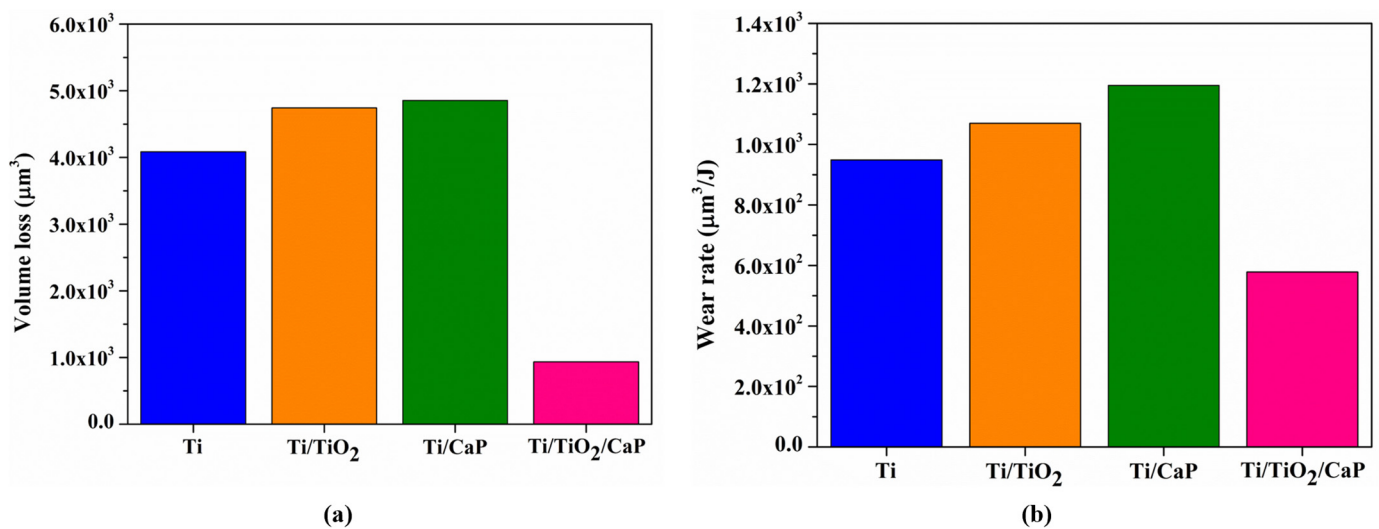
Figure 13. (**a**) Volume loss of wear track (**b**) Wear rate after tribocorrosion test.

Figure 13b shows the worn rate that corroborates with the perspective of the synergic corrosion effect. The wear rate result demonstrated the impact of wear on the degradations of titanium materials coated with both TiO_2 and CaP decreasing significantly. The wear rate decrease is proportional to both contributions of dissipated energy and lower CR.

In the tribocorrosion tests, it can be observed that the Ti sample shows 948.92 μm^3/J. It is related to the Ti/TiO_2 and Ti/CaP, which show 1069.93 μm^3/J and 1195.13 μm^3/J, respectively. Double-coated Ti/TiO_2/CaP presents the lower Wr with 578.45 μm^3/J, indicating the protective action in both degradation mechanisms, electrochemical and wear. These results suggest that applying the double-coating technique improves the tribocorrosion resistance of commercial titanium. This is quite probably a result of the low hardness of Ti/TiO_2/CaP which enables the formation of a smooth layer that functions as a lubricant between the interface and the counterpart. This layer significantly enhances the biomaterial's lifecycle after implantation by minimizing solution percolation in the titanium bulk caused by superficial cracks and reducing wear damage [56].

4. Conclusions

Three different coating configurations have been produced by electrochemical procedures based on the self-oxidation of titanium substrate and the reduction of calcium phosphate isolates or combined in a two-step deposition. The coatings proposed improved electrochemical and tribological properties. Furthermore, the combination of Titanium oxide as an intermediate layer to the deposition of calcium phosphate species promoted a significant increase in the protection of the substrate. The Ti/TiO_2/CaP achieves 99.93% protection in static experiments and significantly decreases corrosion contribution during tribocorrosion tests in SBF. The tribocorrosion experiments demonstrated that the use of TiO_2/CaP decreased in tribological parameters with COF 0.25, *P* with 1.62 J, and Wr with 578.45 μm^3/J, all values better among the analyzed groups. This deposition approach is suitable for future biomedical applications.

Author Contributions: A.S. and J.T.: Conceptualization, investigation, data curation, formal analysis, methodology, writing—original draft, and writing—review and editing. C.F.: Design tribometer and experiments of wear, conceptualization, resources, data curation, formal analysis, investigation, and writing—review and editing. E.R. and N.C.: Resources, data curation, investigation, and writing—review and editing. P.N.L.-F.: Conceptualization, funding acquisition, project administration, resources, supervision, validation, formal analysis, and writing—review and editing. All authors have read and agreed to the published version of the manuscript.

References

1. Juechter, V.; Franke, M.; Merenda, T.; Stich, A.; Körner, C.; Singer, R. Additive manufacturing of Ti-45Al-4Nb-C by selective electron beam melting for automotive applications. *Addit. Manuf.* **2018**, *22*, 118–126. [CrossRef]
2. Tan, Z.-Q.; Zhang, Q.; Guo, X.-Y.; Zhao, W.-J.; Zhou, C.-S.; Liu, Y. New development of powder metallurgy in automotive industry. *J. Cent. South Univ.* **2020**, *27*, 1611–1623. [CrossRef]
3. Williams, J.C.; Boyer, R.R. Opportunities and Issues in the Application of Titanium Alloys for Aerospace Components. *Metals* **2020**, *10*, 705. [CrossRef]
4. Tang, H.; Tao, W.; Wang, H.; Song, Y.; Jian, X.; Yin, L.; Wang, X.; Scarpa, F. High-performance infrared emissivity of micro-arc oxidation coatings formed on titanium alloy for aerospace applications. *Int. J. Appl. Ceram. Technol.* **2017**, *15*, 579–591. [CrossRef]
5. Hatt, O.; Lomas, Z.; Thomas, M.; Jackson, M. The effect of titanium alloy chemistry on machining induced tool crater wear characteristics. *Wear* **2018**, *408–409*, 200–207. [CrossRef]
6. Hall, D.J.; Pourzal, R.; Lundberg, H.J.; Mathew, M.T.; Jacobs, J.J.; Urban, R.M. Mechanical, chemical and biological damage modes within head-neck tapers of CoCrMo and Ti6Al4V contemporary hip replacements. *J. Biomed. Mater. Res. Part B Appl. Biomater.* **2017**, *106*, 1672–1685. [CrossRef]
7. Liu, J.; Wang, R.; Wang, H.; Wang, Y.; Lv, D.; Diao, P.; Feng, S.; Gao, Y. Biomechanical Comparison of a New Memory Compression Alloy Plate versus Traditional Titanium Plate for Anterior Cervical Discectomy and Fusion: A Finite Element Analysis. *BioMed Res. Int.* **2020**, *2020*, 5769293. [CrossRef]
8. Nicholson, J.W. Titanium Alloys for Dental Implants: A Review. *Prosthesis* **2020**, *2*, 100–116. [CrossRef]
9. Çaha, I.; Alves, A.; Affonço, L.; Lisboa-Filho, P.; da Silva, J.H.D.; Rocha, L.; Pinto, A.; Toptan, F. Corrosion and tribocorrosion behaviour of titanium nitride thin films grown on titanium under different deposition times. *Surf. Coat. Technol.* **2019**, *374*, 878–888. [CrossRef]
10. Gao, A.; Hang, R.; Bai, L.; Tang, B.; Chu, P.K. Electrochemical surface engineering of titanium-based alloys for biomedical application. *Electrochim. Acta* **2018**, *271*, 699–718. [CrossRef]
11. Çaha, I.; Alves, A.; Affonço, L.; da Silva, J.; Rodrigues, I.; Grandini, C.; Rocha, L.; Pinto, A.; Lisboa-Filho, P.; Toptan, F. Degradation behaviour of Ti-12Nb alloy coated with ZnO/TiN double layer. *Surf. Coat. Technol.* **2021**, *413*, 127104. [CrossRef]
12. Trino, L.D.; Dias, L.F.; Albano, L.G.; Bronze-Uhle, E.S.; Rangel, E.C.; Graeff, C.F.; Lisboa-Filho, P.N. Zinc oxide surface functionalization and related effects on corrosion resistance of titanium implants. *Ceram. Int.* **2018**, *44*, 4000–4008. [CrossRef]
13. Fazel, M.; Salimijazi, H.R.; Shamanian, M. Improvement of Corrosion and Tribocorrosion Behavior of Pure Titanium by Subzero Anodic Spark Oxidation. *ACS Appl. Mater. Interfaces* **2018**, *10*, 15281–15287. [CrossRef] [PubMed]
14. Zhang, X.; Wu, Y.; Lv, Y.; Yu, Y.; Dong, Z. Formation mechanism, corrosion behaviour and biological property of hydroxyapatite/TiO$_2$ coatings fabricated by plasma electrolytic oxidation. *Surf. Coat. Technol.* **2020**, *386*, 125483. [CrossRef]
15. Capellato, P.; Sachs, D.; Vilela, F.B.; Melo, M.M.; Silva, G.; Rodrigues, G.; Zavaglia, C.A.D.C.; Nakazato, R.Z.; Claro, A.P.R.A. Influence of Annealing Temperature on Corrosion Resistance of TiO$_2$ Nanotubes Grown on Ti–30Ta Alloy. *Metals* **2020**, *10*, 1106. [CrossRef]
16. Fontes, A.C.C.A.; Sopchenski, L.; Laurindo, C.A.H.; Torres, R.D.; Popat, K.C.; Soares, P. Annealing Temperature Effect on Tribocorrosion and Biocompatibility Properties of TiO$_2$ Nanotubes. *J. Bio Tribo-Corros.* **2020**, *6*, 64. [CrossRef]
17. Ishikawa, K.; Garskaite, E.; Kareiva, A. Sol–gel synthesis of calcium phosphate-based biomaterials—A review of environmentally benign, simple, and effective synthesis routes. *J. Sol-Gel. Sci. Technol.* **2020**, *94*, 551–572. [CrossRef]
18. Lu, J.; Yu, H.; Chen, C. Biological properties of calcium phosphate biomaterials for bone repair: A review. *RSC Adv.* **2018**, *8*, 2015–2033. [CrossRef]
19. Tohidi, P.M.S.; Safavi, M.S.; Etminanfar, M.; Khalil-Allafi, J. Pulsed electrodeposition of compact, corrosion resistant, and bioactive HAp coatings by application of optimized magnetic field. *Mater. Chem. Phys.* **2020**, *254*, 123511. [CrossRef]

20. Zhang, X.; Lv, Y.; Fu, S.; Wu, Y.; Lu, X.; Yang, L.; Liu, H.; Dong, Z. Synthesis, microstructure, anti-corrosion property and biological performances of Mn-incorporated Ca-P/TiO$_2$ composite coating fabricated via micro-arc oxidation. *Mater. Sci. Eng. C* **2020**, *117*, 111321. [CrossRef]

21. Sheykholeslami, S.O.R.; Khalil-Allafi, J.; Fathyunes, L. Preparation, Characterization, and Corrosion Behavior of Calcium Phosphate Coating Electrodeposited on the Modified Nanoporous Surface of NiTi Alloy for Biomedical Applications. *Met. Mater. Trans. A* **2018**, *49*, 5878–5887. [CrossRef]

22. Costa, A.; Sousa, L.; Alves, A.; Toptan, F. Tribocorrosion behaviour of bio-functionalized porous Ti surfaces obtained by two-step anodic treatment. *Corros. Sci.* **2020**, *166*, 108467. [CrossRef]

23. Ramalho, A.; Miranda, J.C. The relationship between wear and dissipated energy in sliding systems. *Wear* **2006**, *260*, 361–367. [CrossRef]

24. Huq, M.; Celis, J.-P. Expressing wear rate in sliding contacts based on dissipated energy. *Wear* **2002**, *252*, 375–383. [CrossRef]

25. Abdo, J. Materials Sliding Wear Model Based on Energy Dissipation. *Mech. Adv. Mater. Struct.* **2014**, *22*, 298–304. [CrossRef]

26. Jahangiri, M.; Hashempour, M.; Razavizadeh, H.; Rezaie, H. Application and conceptual explanation of an energy-based approach for the modelling and prediction of sliding wear. *Wear* **2012**, *274–275*, 168–174. [CrossRef]

27. Jahangiri, M.; Hashempour, M.; Razavizadeh, H.; Rezaie, H. A new method to investigate the sliding wear behaviour of materials based on energy dissipation: W–25 wt% Cu composite. *Wear* **2012**, *274–275*, 175–182. [CrossRef]

28. Vieira, A.; Ribeiro, A.; Rocha, L.; Celis, J. Influence of pH and corrosion inhibitors on the tribocorrosion of titanium in artificial saliva. *Wear* **2006**, *261*, 994–1001. [CrossRef]

29. Zakir, O.; Idouhli, R.; Elyaagoubi, M.; Khadiri, M.; Aityoub, A.; Koumya, Y.; Rafqah, S.; Abouelfida, A.; Outzourhit, A. Fabrication of TiO$_2$ Nanotube by Electrochemical Anodization: Toward Photocatalytic Application. *J. Nanomater.* **2020**, *2020*, 4745726. [CrossRef]

30. Çomaklı, O.; Yazıcı, M.; Yetim, T.; Yetim, A.; Çelik, A. Effect of Ti amount on wear and corrosion properties of Ti-doped Al$_2$O$_3$ nanocomposite ceramic coated CP titanium implant material. *Ceram. Int.* **2018**, *44*, 7421–7428. [CrossRef]

31. Li, Y.; Su, K.; Bai, P.; Wu, L. Microstructure and property characterization of Ti/TiBCN reinforced Ti based composite coatings fabricated by laser cladding with different scanning speed. *Mater. Charact.* **2019**, *159*, 110023. [CrossRef]

32. Li, T.-T.; Ling, L.; Lin, M.-C.; Peng, H.-K.; Ren, H.-T.; Lou, C.-W.; Lin, J.-H. Recent advances in multifunctional hydroxyapatite coating by electrochemical deposition. *J. Mater. Sci.* **2020**, *55*, 6352–6374. [CrossRef]

33. Schmidt, R.; Gebert, A.; Schumacher, M.; Hoffmann, V.; Voss, A.; Pilz, S.; Uhlemann, M.; Lode, A.; Gelinsky, M. Electrodeposition of Sr-substituted hydroxyapatite on low modulus beta-type Ti-45Nb and effect on in vitro Sr release and cell response. *Mater. Sci. Eng. C* **2019**, *108*, 110425. [CrossRef]

34. Vidal, E.; Buxadera-Palomero, J.; Pierre, C.; Manero, J.M.; Ginebra, M.-P.; Cazalbou, S.; Combes, C.; Rupérez, E.; Rodríguez, D. Single-step pulsed electrodeposition of calcium phosphate coatings on titanium for drug delivery. *Surf. Coat. Technol.* **2018**, *358*, 266–275. [CrossRef]

35. Gopi, D.; Indira, J.; Kavitha, L. A comparative study on the direct and pulsed current electrodeposition of hydroxyapatite coatings on surgical grade stainless steel. *Surf. Coat. Technol.* **2012**, *206*, 2859–2869. [CrossRef]

36. Mokabber, T.; Zhou, Q.; Vakis, A.; van Rijn, P.; Pei, Y. Mechanical and biological properties of electrodeposited calcium phosphate coatings. *Mater. Sci. Eng. C* **2019**, *100*, 475–484. [CrossRef]

37. Singh, J.; Chatha, S.S.; Singh, H. Characterization and corrosion behavior of plasma sprayed calcium silicate reinforced hydroxyapatite composite coatings for medical implant applications. *Ceram. Int.* **2020**, *47*, 782–792. [CrossRef]

38. Fathyunes, L.; Khalil-Allafi, J.; Moosavifar, M. Development of graphene oxide/calcium phosphate coating by pulse electrodeposition on anodized titanium: Biocorrosion and mechanical behavior. *J. Mech. Behav. Biomed. Mater.* **2018**, *90*, 575–586. [CrossRef]

39. Behera, R.; Das, A.; Pamu, D.; Pandey, L.; Sankar, M. Mechano-tribological properties and in vitro bioactivity of biphasic calcium phosphate coating on Ti-6Al-4V. *J. Mech. Behav. Biomed. Mater.* **2018**, *86*, 143–157. [CrossRef]

40. Pavlović, M.R.P.; Eraković, S.G.; Pavlović, M.M.; Stevanović, J.S.; Panić, V.V.; Ignjatović, N.L. Anaphoretical/oxidative approach to the in-situ synthesis of adherent hydroxyapatite/titanium oxide composite coatings on titanium. *Surf. Coat. Technol.* **2018**, *358*, 688–694. [CrossRef]

41. Shahmohammadi, P.; Khazaei, B.A. Characterization of Zn/Mg-enriched calcium phosphate coating produced by the two-step pulsed electrodeposition method on titanium substrate. *Surf. Interfaces* **2020**, *22*, 100819. [CrossRef]

42. Liu, B.; Yu, W.-L.; Xiao, G.-Y.; Chen, C.-Z.; Lu, Y.-P. Comparative investigation of hydroxyapatite coatings formed on titanium via phosphate chemical conversion. *Surf. Coat. Technol.* **2021**, *413*, 127093. [CrossRef]

43. Ramachandran, R.; Nosonovsky, M. Coupling of surface energy with electric potential makes superhydrophobic surfaces corrosion-resistant. *Phys. Chem. Chem. Phys.* **2015**, *17*, 24988–24997. [CrossRef] [PubMed]

44. Rosales-Leal, J.; Rodríguez-Valverde, M.; Mazzaglia, G.; Ramón-Torregrosa, P.; Díaz-Rodríguez, L.; García-Martínez, O.; Vallecillo-Capilla, M.; Ruiz, C.; Cabrerizo-Vílchez, M. Effect of roughness, wettability and morphology of engineered titanium surfaces on osteoblast-like cell adhesion. *Colloids Surf. A Physicochem. Eng. Asp.* **2010**, *365*, 222–229. [CrossRef]

45. Katić, J.; Šarić, A.; Despotović, I.; Matijaković, N.; Petković, M.; Petrović, Ž. Bioactive Coating on Titanium Dental Implants for Improved Anticorrosion Protection: A Combined Experimental and Theoretical Study. *Coatings* **2019**, *9*, 612. [CrossRef]

46. Singh, S.; Pandey, K.K.; Islam, A.; Keshri, A.K. Corrosion behaviour of plasma sprayed graphene nanoplatelets reinforced hydroxyapatite composite coatings in simulated body fluid. *Ceram. Int.* **2020**, *46*, 13539–13548. [CrossRef]
47. Si, Y.; Liu, H.; Yu, H.; Jiang, X.; Sun, D. A heterogeneous TiO_2/$SrTiO_3$ coating on titanium alloy with excellent photocatalytic antibacterial, osteogenesis and tribocorrosion properties. *Surf. Coat. Technol.* **2021**, *431*, 128008. [CrossRef]
48. Maleki-Ghaleh, H.; Khalil-Allafi, J. Effect of hydroxyapatite-titanium-MWCNTs composite coating fabricated by electrophoretic deposition on corrosion and cellular behavior of NiTi alloy. *Mater. Corros.* **2019**, *70*, 2128–2138. [CrossRef]
49. Messous, R.; Henriques, B.; Bousbaa, H.; Silva, F.S.; Teughels, W.; Souza, J.C.M. Cytotoxic effects of submicron- and nano-scale titanium debris released from dental implants: An integrative review. *Clin. Oral Investig.* **2021**, *25*, 1627–1640. [CrossRef]
50. Zhou, Z.; Shi, Q.; Wang, J.; Chen, X.; Hao, Y.; Zhang, Y.; Wang, X. The unfavorable role of titanium particles released from dental implants. *Nanotheranostics* **2021**, *5*, 321–332. [CrossRef]
51. Ramachandran, R.A.; Barão, V.A.R.; Matos, A.O.; Cordeiro, J.M.; Grandini, C.R.; Sukotjo, C.; Mathew, M.T. Suitability of Ti–Zr Alloy for Dental Implants: Tribocorrosion Investigation. *J. Bio Tribo-Corros.* **2021**, *7*, 152. [CrossRef]
52. Sousa, L.; Basilio, L.; Alves, A.; Toptan, F. Tribocorrosion-resistant biofunctionalized Ti-Al_2O_3 composites. *Surf. Coat. Technol.* **2021**, *420*, 127329. [CrossRef]
53. Blau, P.J. The significance and use of the friction coefficient. *Tribol. Int.* **2001**, *34*, 585–591. [CrossRef]
54. Sousa, L.; Mendes, A.R.; Pinto, A.M.P.; Toptan, F.; Alves, A.C. Influence of Calcium Acetate Concentration in Electrolyte on Tribocorrosion Behaviour of MAO Treated Titanium. *Metals* **2021**, *11*, 1985. [CrossRef]
55. Semetse, L.; Obadele, B.; Raganya, L.; Geringer, J.; Olubambi, P.A. Fretting corrosion behaviour of Ti-6Al-4V reinforced with zirconia in foetal bovine serum. *J. Mech. Behav. Biomed. Mater.* **2019**, *100*, 103392. [CrossRef] [PubMed]
56. Cai, F.; Zhou, Q.; Chen, J.; Zhang, S. Effect of inserting the Zr layers on the tribo-corrosion behavior of Zr/ZrN multilayer coatings on titanium alloys. *Corros. Sci.* **2023**, *213*, 111002. [CrossRef]